Oxygen Reduction Kinetics in Low and Medium Temperature Acid Environment: Correlation of Water Activation and Surface Properties in Supported Pt and Pt Alloy Electrocatalysts

Vivek S. Murthi, R. Craig Urian,† and Sanjeev Mukerjee*

Department of Chemistry, Northeastern University, 360 Huntington Avenue, Boston, Massachusetts 02115

Received: March 5, 2004; In Final Form: April 20, 2004

Kinetics of oxygen reduction reaction on supported Pt and several Pt alloy electrocatalysts (PtCo/C and PtFe/C) have been investigated in terms of the effect of alloying on the initiation and extent of surface oxide formation (water activation: $xH_2O + Pt^*(M) \rightarrow (M)Pt-[OH]_x + xH^+ + xe^-$). For this, a systematic RRDE investigation has been conducted in trifluoromethane sulfonic acid (TFMSA) as a function of concentration (in the range 1 to 6 M) which corresponds to a change in mole ratio of water/acid from 50:1 in 1 M to 4:1 in 6 M TFMSA. This change in relative amount of water in the various concentrations can also be indirectly correlated to the relative humidity in an operating PEM fuel cell. The scope of this effort was (a) to confirm the shift and lowering of water activation on supported Pt alloy electrocatalysts relative to Pt at lower concentrations (1 M); (b) to compare the inherent activity for ORR on supported Pt and Pt alloy nanoparticles without the effect of oxide formation via activation of water, this was enabled at higher concentrations of TFMSA (6 M); (c) to relate the activation energy values at 1 M for Pt and Pt alloy electrocatalysts for further insight into the nature of the rate-determining step in the mechanism; and (d) to examine the relative formation of peroxides via a parallel pathway for Pt and Pt alloy electrocatalysts in 1 and 6 M TFMSA. Our results confirm that for fully hydrated systems akin to 1 M concentration the alloys shift the formation and extent of water activation on the Pt alloy surfaces; this has been correlated with in-situ XAS data (changes to Pt electronic states and short-range atomic order) as well as via direct EXAFS probe of the formation of oxygenated species above 0.75 V (typical potential for initiation of surface oxides on Pt). The lowering of oxide formation agrees well with the extent of enhancement of ORR activity. Activation energy determinations at 1 M concentration however revealed no difference between Pt and Pt alloys, indicating thereby that the rate-limiting step remains unchanged. At lower water activity (6 M) with negligible water activation (and hence surface oxides), the Pt surface was found to possess a higher activity for ORR as compared to the alloys. In addition, the determination of peroxide yield on the Pt surface showed that there was variation both in terms of alloy formation as well as the water activity at the interface. All these results have been discussed in the context of a PEM fuel cell operating in the low to medium temperature range (70−120 °C) and humidity variation (100 to 10%).

Introduction

Proton-exchange-membrane fuel cells (PEMFC) with their higher efficiency, low heat and noise signature, fuel flexibility, continuous operation, and modularity are an attractive choice over competitors such as batteries and internal combustion engines for portable and stand-alone power generation. From a systems standpoint, one of the primary technical challenges common to both reformer-based and direct methanol low and medium temperature PEMFC's is the large overpotential loss as well as the generally poor kinetics of the ORR. This results in a typical loss of approximately 220 mV at or near the open circuit potential (OCP) with the current state-of-the-art low Pt loading electrodes (0.1 to 0.2 mg/cm^2). Hence performance levels do not exceed 0.2 to 0.3 A/cm^2 at 0.8 V (reformate air operation at 80 °C, ambient pressure) with the current state-of-the-art supported Pt (Pt/C) electrocatalysts. Since every 20 mV lowering of the ORR overpotential loss means approximately 2-fold increment in current density, the incentive for further improvement in the ORR electrocatalysis is significant. Prior research has shown that a 50−60 mV lowering of the overpotential loss for ORR is possible.[1−5] This could enable a doubling of the PEMFC stack performance level from the current state-of-the-art 1 kW/L[6] to 2 kW/L.

The principal causes of the poor kinetics of the four-electron oxygen reduction reaction can be attributed mainly to the relatively high overpotential losses in the low current density region of the oxygen reduction reaction.[7,8] The high cathodic overpotential loss of ∼220 mV is attributed to a mixed potential that is set up at the oxygen electrode due to a combination of slow O_2-reduction kinetics and competing anodic process such as Pt-oxide formation and/or impurity oxidation.[9] Further, the low exchange current density of the O_2-reduction reaction results in a semi-exponential Tafel-like behavior, indicating that the reaction is activation controlled over 3 orders of magnitude in current density. It has been determined that the exchange current density of O_2-reduction is 5−6 orders of magnitude lower than

* Corresponding author. Phone: 617 373 2382. Fax: 617 373 8949. E-mail: s.mukerjee@neu.edu.

† Present address: Integrated Fuel Cell Technologies Inc., Burlington, MA.

10.1021/jp048985k CCC: $27.50
Published on Web 06/23/2004

that of the H_2-reduction reaction.[8,10] Since the activation overpotential stretches over 3 orders of magnitude in current density, the problem of significant improvement in O_2-reduction activity is primarily electrocatalytic. The current state-of-the-art PEMFC performance reflects a wealth of previous efforts at improving the electrocatalyst utilization at the electrode−electrolyte interface, making low Pt loadings of ~0.15 mg/cm^2 a reality.[11]

In terms of electrocatalysis, O_2-reduction on Pt crystallites occurs by a parallel mechanism with direct four-electron reduction as the dominant step.[12] However due to large number of possible steps within this ambit, a detailed mechanism still defies formulation. From a mechanistic perspective there are two views regarding the first reaction step. The first view, based on an early proposition by Damjanovic et al.[13] suggested a simultaneous proton and charge-transfer step involving: $O_2 \leftrightarrow O_2$ (ads), followed by a rate-determining charge-transfer step: O_2 (ads) + H^+ + e^- → product(s). This mechanism was supported by results on bulk planar Pt electrodes based on pH and pressure dependencies. Langmuirian kinetics was used to explain the Tafel slope of 120 mV/decade below 0.8 V, while the 60 mV/decade Tafel slope beyond 0.8 V was explained assuming oxygen adsorption under Temkin conditions in the presence of surface Pt−OH poison. One of the key features of this mechanism is the association of the low Tafel slope of 60 mV/decade to the surface Pt−OH, a surface poison to the O_2 adsorption. A second view, proposed by Yeager and co-workers,[14−16] suggests that the most likely mechanism of the four-electron oxygen reduction on Pt involves dissociative chemisorption of an O_2 molecule on a Pt surface. This probably occurs with simultaneous charge transfer. On the basis of the experimental evidence in support of this proposition two routes were suggested;[14,15,17] the primary difference between them is that route I involves a single Pt atom, whereas in route II adjacent sites on two different Pt atoms are involved. In this context it is important to point out that three different models for adsorbed oxygen on metal sites have been proposed: (a) a molecular edge-wise adsorption without rupture of the O═O bond (Griffiths model)—here the bond is formed mainly between the π-orbital of O_2 and an empty d_z^2 orbital on the metal surface with a π-back-bonding to form partially filled d_{xy} and d_{yz} orbitals of the metal and a π^* antibonding orbital of O_2; (b) end-on adsorption through a single bond (Pauling model), in a σ-type bond in which σ-orbitals of O_2 donate electron density to an acceptor d_z^2 orbital on the metal; (c) a bridge model, where we have two bonds with two sites as proposed by Yeager.[18]

Previous reports have shown that the formation of Pt−OH beyond 0.8 V is derived not from the interaction of O_2 with Pt, but rather from reaction of H_2O with Pt causing inhibition of the O_2-reduction[19−21] resulting in a low Tafel slope of 60 mV/decade. In electrolytes containing phosphate or bisulfate anions a low Tafel slope was not observed on Pt(111) due to the surface poisoning of these anions which shift the Pt−OH formation to a more positive potential.[20,22] However, for the other low index planes Pt(100) and Pt(110) a change of slope was observed since the anion adsorption on these planes is minimal.[23] Significant improvement of ORR electrocatalysis could therefore be afforded by, first inhibiting the formation of adsorbed oxygenated species (primarily Pt−OH) beyond 0.8 V, a known surface poison, and, second, changing the electronic and short-range atomic order around Pt to induce alternative lower energy pathways for improved ORR kinetics.

Many Pt-based transition metal alloys have been suggested for use as a cathode catalyst,[1,24,25] they have shown varying degrees of enhancement as compared to Pt in a completely hydrated PEM fuel cell. Changes in short-range atomic order, particle size, Pt *d*-band vacancy, Pt skin effects, and Pt−OH inhibition have been advanced as some of the reasons attributed for the enhanced performance by these alloys.[26−29] For further details see reviews by Adzic[12] and Mukerjee.[30]

Inhibiting or shifting the onset potential (approximately 800 mV vs RHE for Pt) of Pt−OH formation, providing free sites for molecular oxygen adsorption, is generally expected to lower the overpotential losses. A number of prior reports have provided indirect evidence to the possibility of inhibiting the formation of anodic activation of water for Pt−OH formation.[2,3,31,32] Shifting the onset potential of OH formation on Pt is dependent on (a) the ability of the alloying elements to modify the Pt electronic and short-range atomic order for inhibiting activation of H_2O and (b) the ability of the alloying element to attract and hold H_2O_{ads} more strongly than the surrounding surface Pt atoms.

The effect of different electrolytes for ORR has been extensively investigated.[16,17] As a part of these investigations, trifluoromethane sulfonic acid (TFMSA) was studied initially in an effort to identify an alternate electrolyte medium for a phosphoric acid fuel cell (PAFC). This was motivated by problems of strong phosphate anion adsorption on Pt,[33] as well as poor proton conductivity and oxygen solubility, typically encountered in concentrated phosphoric acid. Trifluoromethane sulfonic acid (TFMSA) and other analogous sulfonic acids significantly alleviated all these aforementioned problems thereby enabling increased ORR activity. Notable among these prior investigations are those by Enayetullah and co-workers[34] who have studied oxygen reduction (ORR) electrocatalysis on a polycrystalline (pc) Pt microelectrode in various concentrations of TFMSA. Significant enhancement of ORR activity was reported as a consequence of the use of TFMSA rather than another acid. In this investigation, higher Tafel slope ~ $2RT/F$ or 120 mV/decade was reported in high concentrations of TFMSA (greater than 6 M) which was attributed to the lower activity of water. They concluded that the high ORR activity in concentrated TFMSA was a consequence of an oxide-free Pt surface under conditions of low water activity. Similar results were also shown with trifluoroacetic acid with the potassium salt of trifluoroacetate as electrolyte with varying mole ratio of water.[31]

The parallel pathway for the ORR leading to simultaneous formation of peroxide (two-electron reduction) at the electrocatalyst interface has been reported previously.[35−37] Prior results by Arvia et al.,[35,36] in 0.1 and 1 M TFMSA on faceted Pt single crystals showed dependence on crystal structure for both four-electron oxygen reduction as well as two-electron peroxide formation. This prior report, based on a rotating ring-disk method, showed that higher amounts of peroxide were formed on Pt(100) as compared to Pt(111) and polycrystalline Pt. Prior reports[38−40] have shown increasing peroxide yield at higher overpotentials. A Tafel slope of 165 mV/decade on the (100) crystal plane of Pt in the high overpotential region was explained on the basis of a stronger peroxide adsorption. Recent results by Ross and co-workers[37] have compared peroxide formation of supported Pt alloys relative to Pt/C in 0.1 M $HClO_4$ using a thin film RRDE method. Comparison of Pt−Co/C, Pt−Ni/C (25 a/o) with Pt/C, showed no differences in the peroxide yield.[37] A 50 atomic percent Pt−Ni/C however showed a higher peroxide yield as compared to Pt−Co (same alloying ratio) and Pt/C,[37] thereby offering a tentative possibility of perturbing the parallel pathway for ORR.

One of the main obstacles to getting an insight into the reaction pathway for oxygen reduction is that a lot of variables remain undetermined. Even with the vast knowledge of measured parameters, some rate constants cannot be determined with ring-disk measurements. Inhibition of O_2 reduction at underpotential-deposited (UPD) silver adatoms on Pt was used by Adzic and co-workers to show that the adsorption of O_2 on Pt occurred through a bridge configuration.[41] A more general scheme proposed by Anastasijevic et al.[42] from the analysis of data from ring-disk experiments included most of the possible intermediates and were able to explain both the "series" and "parallel" pathways for ORR.

Investigation of peroxide formation at the electrocatalyst−ionomer interface in a PEM fuel cell context is especially important from the perspective of attempts to develop alternative proton-conducting polymer membranes capable of elevated temperature operation (120 to 140 °C). The current state-of-the-art perfluorinated systems, such as Nafion, are restricted to operating temperatures below 100 °C. Elevated temperature operation offers better ability to tolerate CO from the reformer feed and better thermal and water management enabling easier system integration. However most of these alternative polymer membranes possess non-fluorinated backbones and pendant chains which are susceptible to attack by free radicals. Among the possible mechanisms postulated are the following: (a) oxygen diffusing through the membrane to the anode and forming $HOO^{\bullet}$ radicals at the surface of the catalyst leading to an attack of the tertiary H at the α carbon of the polymer;[43] (b) oxygen reduction at the cathode proceeding through a peroxide intermediate H_2O_2, either reacting directly or via trace metal ions in the membrane to form $HOO^{\bullet}$ and $HO^{\bullet}$ radicals, causing membrane degradation during the cathode reaction.[43] Hence the determination of the peroxide yield is important from the perspective of the different electrocatalysts (Pt and Pt alloys) and water activity at the interface.

The objective of this investigation is to examine (a) the inherent activity for oxygen reduction on select Pt alloy electrocatalysts relative to Pt, and (b) the peroxide yield at the electrocatalyst−ionomer interface. Both parts of this investigation are related to the effect of variation of water activity at the interface, which is achieved by varying the concentration of TFMSA,[44] an electrolyte with low susceptibility for anion adsorption[45,46] and excellent transport properties for protons and dissolved oxygen.[14,15,17,18,47] By varying the activity of water at the interface, it is therefore possible to control the extent of anodic water activation and hence formation of oxide species on the electrocatalyst surface. These have been reported previously by Conway et al.[48]and Enayetullah et. al.[49] This is used in this investigation to understand the inherent activity of select Pt alloys (PtCo/C and PtFe/C) for oxygen reduction. By curtailing the influence of surface oxides on oxygen reduction, effects of the perturbation of the electronic and short-range atomic order (Pt−Pt bond distance and coordination number) of Pt as a result of alloying can be determined. Formation of peroxides at the interface is also dependent on the presence of water; hence controlling the water activity at the interface is expected to provide important insight on the role of the electrocatalyst surface properties (electronic and short-range character) and its relation to the extent of two-electron peroxide formation.

Experimental Section

Electrocatalyst. Two different carbon-supported binary Pt alloys, PtFe/C and PtCo/C, with a nominal composition of 3:1 (Pt/M) atomic ratio were investigated with Pt/C used as a control. All electrocatalysts were prepared in-house and had a metal loading of 20% on carbon support (Vulcan XC-72, Cabot, USA). The preparation methodology used[50−53] was the well-known colloidal "sol" and carbothermic reduction methods. Briefly, the preparation method involved initial preparation of a Pt/C sample using a sulfato-complex approach described in more detail elsewhere.[30,53,54] The incorporation of the second alloying element was accomplished by first dispersing the supported electrocatalyst in an aqueous medium and raising the pH to 8 by the addition of ammonium hydroxide. Next, the appropriate salt solution of the alloying element was added and the pH reduced to around 5, followed by drying and carbothermic reduction in an inert atmosphere at 900 °C. In these methods, an oxide of the second alloying element is incorporated on the supported Pt/C electrocatalyst. When this is subjected to carbothermic reduction under inert conditions at 900 °C, the crystallites undergo reduction and alloying on the carbon support, thus providing for supported alloy nanoparticles.

All electrochemical measurements were made at room temperature using a rotating ring-disk electrode setup from Pine Instruments connected to an Autolab (Ecochemie Inc., model-PGSTAT 30) potentiostat equipped with a bipotentiostat interface. All potentials were measured with respect to a sealed hydrogen reference electrode (RHE)[55,56] made from the same concentration of the electrolyte used in the experiment. To avoid potential artifacts caused as a result of different electrolyte concentrations in the reference relative to experiment, the electrolyte in the reference electrode had the same concentration as used in the experiment. Hence, any potential shift (Nernst shift) in the reference electrode due to the concentration of electrolyte is corrected for, and all the CV's recorded at the working electrode are a true reflection of the effect of water activation.

Electrolyte. Trifluoromethane sulfonic acid (CF_3SO_3H/TFMSA) was obtained from 3M Inc., and underwent a purification step as described elsewhere.[34,47,57] TFMSA was triply distilled under vacuum below 60 °C and the monohydrate (9.5 M) was then prepared from the purified acid. The pure monohydrate was then re-crystallized to form a white crystalline solid which was stored in a Teflon bottle for future use. The re-crystallization step was carried out two more times for further purification prior to the preparation of the 6 and 1 M solutions used for this investigation. The solutions were first purged with N_2, and the electrode was cycled continuously until a clean reproducible Pt cyclic voltammetric profile was obtained. The solutions were then purged with O_2 for ORR measurements. Measurements were also made on a 6 mm diameter polycrystalline (pc) Pt disk (Pine Instruments) as a control experiment. The diffusion coefficient of oxygen and its solubility in these solutions were determined by a chronoamperometric method using a Pt microelectrode as reported elsewhere.[58,59]

Electrode Preparation. Suspensions of 1 mg of catalyst per mL in 2-propanol were obtained by ultrasonication for 30 min. A 20 μL volume of 5 wt % Nafion was added to the suspension prior to mixing to act as a binder. Since the amount of catalyst to Nafion loading was very small relative to normal fuel cell electrodes (wt ratio of Pt/C to Nafion was 50:1, mg/cm^2) and comparable to previously reported rotating disk electrode experiments,[60,61] diffusion effects due to the Nafion layer were neglected. A glassy carbon disk electrode (0.283 cm^2, Pine Instruments) was used as the substrate for the supported catalysts and was polished to a mirror finish using 0.05 μm alumina suspension (Buehler) before loading the catalyst. A 20 μL aliquot of the suspension (corresponding to 4 μg of metal) was

then loaded onto the glassy carbon to give a constant metal loading of ~14 μg/cm^2 (geometric) and was allowed to dry before introducing it into the electrolyte. The gold ring electrode was activated prior to any experiment by cycling between 0 and 1.6 V (50 mV/s) in 1 M CF_3SO_3H until steady-state voltammetry was reached.

After preparation, the electrodes were immersed in oxygen-free electrolyte solutions at room temperature and cycled several times between 0 and 1.2 V at 50 mV/s and then cycled further at 10 mV/s; the cyclic voltammograms were then recorded. For oxygen reduction studies the electrode was immersed in oxygen-saturated (Med-Tech Gases Inc.) electrolyte and cycled initially between 0.2 and 1.2 V at 1000 rotations per minute. For ORR experiments the electrode was scanned between 1.2 and 0.3 V at 25 mV/s for 10 cycles at each rotation, and the last 3 scans at each rotation rate were used for data analysis. The rotation rates were 400, 625, 900, 1225, and 1600 rpm, the upper limit was 1600 rpm due to viscosity issues in high concentrations of TFMSA. Kinetic measurements of the ORR in terms of the Tafel parameters and kinetic currents were made, similar to a wealth of prior published approaches for the analysis of the RDE data.[62,63] Use of the ring disk electrode in conjunction with the rotating disk experiments followed well-known methodologies described elsewhere.[61,64,65] Here, the peroxide yield as a result of two-electron reduction was determined in parallel to the overall ORR activity. Kinetic measurements were also performed at different temperatures (30, 40, 50, and 60 °C) to evaluate the activation energy for ORR based on an Arrhenius type of plot.

Physicochemical Characterization. X-ray diffraction was conducted using the high resolution X-18A beam line at the National Synchrotron Light Source (NSLS) at Brookhaven National Laboratory. Previously reported characterization of the 3:1 PtM/C composition[25] showed the existence of a fcc metallic phase with an average particle size of ca. 4 nm. Line broadening analysis of the primary XRD peak ⟨111⟩ was conducted using the Scherrer treatment of the data. The data were first fitted to an indexing program, which allowed accurate measurement of the line widths at half-maximum. These widths were then used to obtain the particle size. Corrections for beam deviations in the instrument were considered negligible due to the high collimation of the synchrotron beam.

XANES (X-ray absorption near-edge structure) data from in-situ X-ray absorption spectroscopy (XAS) was measured. The objective was to verify the nominal atomic ratios as well as nature of alloying, especially in the cases where the difference in the line shifts of the XRD patterns between Pt and Pt alloy electrocatalysts was very small. Further, the Pt *d*-band vacancy/atom was also determined from the relative areas under the Pt L_3 and L_2 edges for all the Pt and Pt alloy compositions. The methodology for analysis of the XANES spectrum followed those of Wong et al.[66] The procedure for determining the Pt *d*-band vacancy concentration was initially developed by Mansour and co-workers[67,68] and its methodology applied to the study of electrocatalysis by Mukerjee et al.[2,3]

A special in-situ spectro-electrochemical cell (described in detail elsewhere[69]) was used, which allowed XAS measurements in transmission mode with the working electrode in a fully flooded state. XAS measurements were conducted at beam line X-11 A at the National Synchrotron Light Source (NSLS) in Brookhaven National Laboratory. Data were collected at both the Pt L (L_3 and L_2) and the alloying element K edges in the transmission mode using an incident, transmission, and reference ion chambers. A Pt foil at the reference detector provided accurate calibration and alignment of the edge positions. Details of the beam line optics and monochromator are given elsewhere.[25] The electrochemical control of the interface was enabled by a digital potentiostat/galvanostat (PGSTSAT 30, Autolab, Echochemie, Brinkmann Instruments). The electrolyte of choice for in-situ XAS measurements was 1 M $HClO_4$. Prior to acquiring the in-situ XAS spectra, electrodes were cycled at least 25 times, between 0.0 and 1.2 V. Since the purpose of the XANES experiment was primarily to determine the atomic ratio of Pt and the alloying element as well as the *d*-band vacancy of Pt/atom, the in-situ spectra were taken at 0.54 V vs RHE. Data collected at this potential were devoid of interference due to adsorbed species, being in the double layer region and close to the potential of zero charge. XAS data was also collected as a function of potential in the range of 0.0 to 1.2 V vs RHE for all the binary alloys in 1 M $HClO_4$. EXAFS analysis on the Pt L_3, Fe and Co K edges followed methodologies developed by Koningsberger et al.,[70,71] the details of which are given elsewhere.[2,3,25,72] Phase and amplitude parameters from standard materials and theoretically calculated values from FEFF6 program using fcc crystal lattice parameters based on appropriate atomic ratios for the PtM alloys were used to fit those from the sample data. The standards used to calculate Pt−Pt and Pt−O interactions were liquid N_2 data for a pure Pt foil and $Na_2Pt(OH)_6$, respectively. A Gaussian pair distribution function (PDF) was used to fit the Pt−Pt and Pt−M (M = Co or Fe). Harmonic thermal vibrations and interatomic PDF's can cause an underestimation of the coordination numbers. A cumulative expansion algorithm which also included the third and fourth terms from an asymmetrical PDF was used as fitting parameters and resulted in a 12 to 19% increase in the coordination numbers relative to the Gaussian PDF. Since, the observed deviations were random and the average bond distances of Pt−Pt and Pt−M increased by 0.02 ± 0.0002 Å, the effect of asymmetry in the samples was considered negligible. Hence, the results reported hereafter are obtained from a Gaussian PDF. The effect of electrolyte environment on the electrocatalyst nanoclusters is not considered here and is the subject of a separate investigation. The use of $HClO_4$ in our in-situ XAS experiments was based on its negligible anion adsorption[22,73] with 1 M concentration, a situation akin to the case with trifluoromethane sulfonic acid.[44,57,74,75]

TABLE 1: Structural Characteristics of the Pt and Pt Alloy Electrocatalyst Using Powder XRD Data at 1.54 Å

electrocatalyst	lattice parameter	Pt−Pt bond distance (Å)	average particle size (Å)
Pt/C	3.927	2.777	25
PtFe/C	3.866	2.733	39
PtCo/C	3.854	2.725	36

Results and Discussion

Characterization of the Nanocluster Size, Crystallinity, and Atomic Parameters: XRD and In-Situ XAS Measurements. The XRD analysis of the electrocatalysts showed a very high degree of crystallinity. Fits of the XRD data to an indexing routine showed that all the patterns (Pt and Pt alloys) corresponded to an fcc lattice. Lattice parameters obtained are given in Table 1. In addition, the Pt−Pt bond distances based on an fcc lattice were calculated on the basis of X-ray line broadening analysis using the Scherrer equation (Table 1). Evidently, alloying of Pt with Fe and Co results in a lowering of the lattice parameters and hence the Pt−Pt bond distances. From a comparison of the XRD pattern with a standard JCPDS database the binary Pt alloys were found to form an intermetallic

TABLE 2: Results of XANES (at Pt L and K edge of alloying metal) and EXAFS Analysis (at the Pt L_3 Edge) for Supported Pt and Pt Alloy Electrocatalysts. All Data Were Measured In-Situ at 0.54 and 0.84 V vs RHE[a]

		Electrode Potential (0.54V vs RHE)			Electrode Potential (0.84V vs RHE)		
electro-catalyst	atomic ratio(a/o) XANES	$(h_j)_{t,s}$ Pt *d*-band vacancy	Pt−Pt (Å)	Pt−Pt (N)	$(h_j)_{t,s}$ Pt *d*-band vacancy	Pt−Pt (Å)	Pt−Pt (N)
Pt/C		0.329	2.77	8.7	0.370	2.77	6.8
PtFe/C	69/31	0.368	2.70	6.7	0.370	2.71	6.5
PtCo/C	72/28	0.401	2.68	6.9	0.390	2.68	7.6

[a] The windows for the Fourier transform parameters used for EXAFS analysis of Pt L_3 edge at 0.54 V are given as follows: Pt/C: $k^n = 3$; Δk (Å^{-1}) = 3.49 − 14.23; Δr (Å) = 1.4 − 3.05. PtCo/C: $k^n = 3$; Δk (Å^{-1}) = 3.22 − 14.61; Δr (Å) = 1.5 − 3.5. PtFe/C: $k^n = 3$; Δk (Å^{-1}) = 3.45 − 17.14; Δr (Å) = 1.5 − 3.4.

crystalline structure with a primary Pt_3M-type superlattice phase with an fcc structure and potential for a secondary PtM-type lattice with a tetragonal structure. The extent of contribution from the secondary phase was estimated by the intensity of the diffraction lines due to the PtM phase (such as (001) and (220) diffraction lines in the PtM/C powder pattern). Contribution from these secondary phases was found to be negligible. The particle size obtained using the Pt(111) diffraction line broadening showed that the alloy catalysts have a particle size somewhat larger than for Pt/C. Table 1 shows that the particle size increases due to alloying [Pt/C < PtCo/C < PtFe/C].

The ratio of Pt:M (alloying elements, Co and Fe) in the electrocatalyst (Table 2) were determined from the edge jumps at the Pt L_3, Co and Fe K edges using the methodologies described elsewhere.[25] It is noteworthy that all the atomic ratios determined by XANES were in excellent agreement with nominal compositions projected from our preparation methodology. The XANES spectra used were measured in-situ at 0.54 V vs RHE. As mentioned earlier in the Experimental Section, the choice of this potential was based on the fact that it is in the middle of the double layer region where the potential interferences from anionic adsorption as well as the usual redox processes associated in the hydrogen and oxygen regions of the voltammograms.

The Pt *d*-band vacancies were derived from analysis of the Pt L_3 and L_2 white lines of XANES. The L_2 and L_3 excitations are due to the transition of $2p_{1/2}$ and $2p_{3/2}$ electrons to the empty Fermi level. Dipole selection rules restrict the orbital angular quantum number transitions to ± 1. Hence a transition of $2p_{3/2}$ to a 5d-orbital is favored. An increase in the L_3 and L_2 whiteline peak is related to changes in *d*-band vacancy and reflects the extent of *d*-band occupancy. A detailed description of this methodology is provided in ref 2 and references therein. The Pt *d*-band occupancies evaluated from the Pt L_3 and L_2 edge curves are given in Table 2 along with the Pt−M atomic ratio. Comparison at 0.54 V vs RHE shows an increase in *d*-band vacancies per atom on alloying, this follows the trend Pt/C < PtFe/C < PtCo/C. This increase in *d*-band character of Pt follows closely with the electron affinity of the alloying metal. XANES also offers the ability to monitor the extent of alloying and the nature of the active surface.

Two sets of Pt alloy catalysts, (i) acid-washed (1 M $HClO_4$ for 48 h, room temperature) and (ii) unwashed PtM/C alloy catalyst, were held at 0.9 V vs RHE and the XANES spectrum was recorded at the Pt L_3 and the M (Co or Fe) K edge for six to 10 hours. The acid wash step followed by washing with deionized water ensures the removal of any non alloyed M metal from the surface of the carbon support prior to electrode fabrication. The XANES analysis at the metal M [Co or Fe] K edge as described elsewhere[54] showed clear evidence of changes in the surface oxidation environment around the alloying elements Fe and Co, when the electrode was polarized at 0.9 V for the unwashed samples. Such a variation in the Fe and Co K edge XANES were however absent for extended durations of up to 9 h with electrode polarized at 0.9 V for the washed electrocatalysts. No changes were detected at the Pt L_3 edge for Pt alloy catalysts polarized (washed and unwashed) with the electrode polarized at 0.9 V for up to 9 h. These results are presented in a separate manuscript.[54] These results using XANES and the stability observations are consistent with the outer layer being pure Pt and the alloying metal further deep in the cluster has been suggested previously.[76] Theoretical calculations of the surface segregation energies of different transition metal alloys by Norskov et al.[77] using a Greens's Function Linear-Muffin-Tin-Orbital (GF-LMTO) calculations combined with a density functional theory (DFT) and coherent potential approximation (CPA) showed a strong antisegregation effect in the case of a PtCo and PtFe alloy where the Co and Fe were considered as solutes in a Pt host. Positive segregation energies of 0.37 and 0.46 eV for Fe and Co, respectively, in a Pt host showed that the Fe and Co atoms prefer to remain in the interior of the alloy. The calculated segregation energies were based on a close packed surface, a system similar to the supported PtM alloys used in our study.

EXAFS Analysis. The first step in the analysis of EXAFS is to extract the normalized EXAFS data from the raw XAS spectrum. After pre-edge subtraction (−200 eV to −50 eV relative to Pt L_3 edge) and post-edge background removal (+50 eV to 1500 eV above the Pt L_3 edge), the EXAFS spectra for supported Pt and Pt alloys were of good quality and underwent further Fourier filtering using windows shown in Table 2. A representative phase corrected forward Fourier transform of the k^3weighted EXAFS (*r*-space) at the Pt L_3 edge for Pt/C and PtCo/C at two potentials 0.54 V and 0.84 V (indicative of a clean region, 0.54 V; and an oxide-covered region, 0.84 V, respectively) are shown in Figures 1a and 1b. Comprehensive EXAFS analysis is typically done following the inverse Fourier transform of the *r*-space to analyze *k*-space amplitudes and to isolate the primary coordination shells of interest. Iterative least-squares fitting using one shell (Pt−Pt) or two shells (Pt−Pt + Pt−O, Pt−Pt + Pt−M) was then carried out on a simplistic model to get unique fits. Thus at 0.54 V, a single-shell (Pt−Pt) fit for Pt/C and a two-shell model (Pt−Pt + Pt−M) fit for Pt−M alloys indicate no Pt−O interactions at this potential. However, at 0.84 V a single-shell model could not fit the data for a Pt/C but a two-shell model (Pt−Pt + Pt−O) derived from a standard sample ($Na_2Pt(OH)_6$ at liq. N_2) could fit the data at this potential. In contrast to this, Pt alloys show no differences due to potential change since the same two-shell model (Pt−Pt + Pt−M) at 0.54 V was able to fit the data at 0.84 V. Further, the effect of alloying on the Pt−Pt bond distances (Table 2) obtained from the EXAFS analysis of the Pt L_3 edge data show a contraction as a result of alloying and follows the same trend as determined by XRD [PtCo/C < PtFe/C < Pt/C]. These Pt−Pt bond distances and the coordination numbers (*N*) obtained for the alloys, Pt−Pt and Pt−M (Table 2) are in good agreement with expected coordination numbers using a cubo-octahedron model described by Benfield.[78] Since the cubo-octahedron model of Benfield correlates overall coordination numbers to particle sizes, there was a good correlation of the data obtained from EXAFS with those obtained from the line broadening analysis

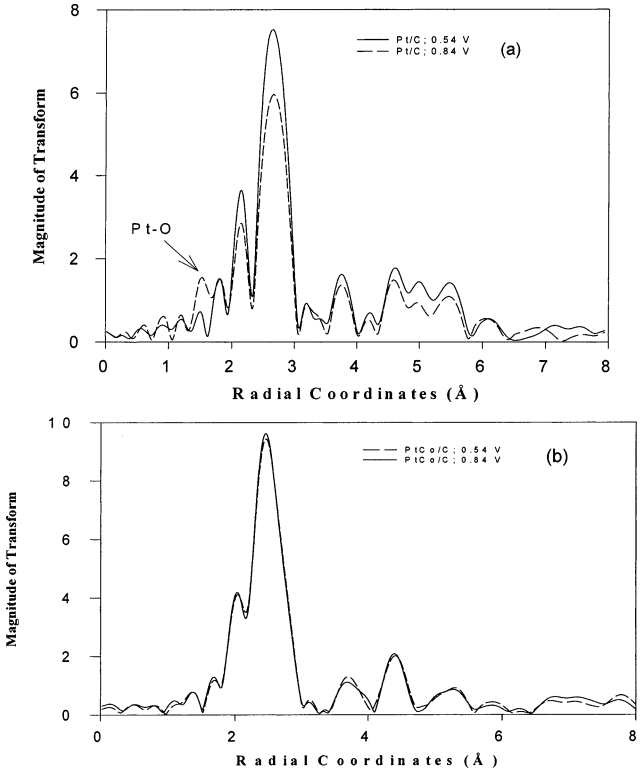

Figure 1. (a) Comparison of k^3 weighted Fourier transform at the Pt L_3 edge (*r* space) measured in-situ at 0.54 V and 0.84 V vs RHE for 20% Pt/C (Fourier filtering windows in Table 2). (b) Comparison of k^3 weighted Fourier transform at the Pt L_3 edge (*r* space) measured in-situ at 0.54 V and 0.84 V vs RHE for PtCo/C (Pt/Co 3:1) (Fourier filtering windows in Table 2).

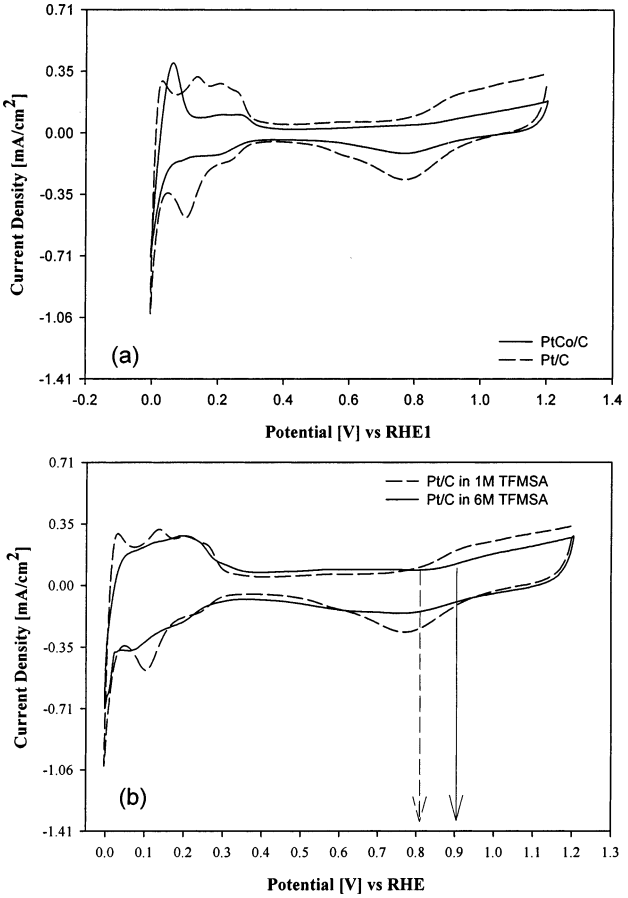

Figure 2. (a) Cyclic voltammograms in oxygen-free 1 M CF_3SO_3H at room temperature for a 20% Pt/C (- -) and a PtCo/C (−) on a glassy carbon (GC) disk electrode at 50 mV/s. Current densities based on geometric electrode area. (b) Cyclic voltammograms for a 20% Pt/C in oxygen-free 1 M (-- -) and 6 M (−) CF_3SO_3H at room temperature at 50 mV/s vs RHE1 and RHE6 reference electrodes, respectively. Current densities based on geometric electrode area.

of XRD. This is indicative of the fact that the electrocatalyst used in this study had an extremely high (close to 100%) degree of crystallinity. This was based on the fact that XRD which only reflects information from diffracting domains (hence systems with long-range order) and EXAFS which probes only short-range atomic order (nearest shell interactions) were in good agreement. The change in *d*-band vacancies (Table 2) for the Pt and Pt alloys during potential transition from 0.54 V (double layer region) to 0.84 V vs RHE (oxide-covered layer) agrees with the EXAFS analysis for Pt/C, and there is an expected increase due to chemisorbed OH species on the surface at 0.84 V relative to 0.54 V; however, such a change is absent for the alloys (Table 2).

Cyclic Voltammetry. Figure 2a shows the steady-state cyclic voltammograms (CV) of a Vulcan XC-72R carbon-supported Pt and PtCo in oxygen-free 1 M trifluoromethane sulfonic acid (CF_3SO_3H) at 50 mV/s with a metal loading of 14 $\mu g_{metal}/cm^2$. The carbon-supported Pt particles possess some degree of low coordinated crystal planes, and hence the hydrogen adsorption/desorption features between 0.4 and 0 V vs RHE are different from the CV expected of a bulk pc-Pt electrode. A comparison of the voltammetry of Pt and PtCo in Figure 2a also shows the difference in the onset of oxide formation on Pt (accepted as Pt−OH) at around 0.7 V vs RHE. PtCo/C exhibits a significantly lower extent of oxide formation. Figure 2b shows the voltammogram on Pt/C in 1 and 6 M CF_3SO_3H at 50 mV/s. It is interesting to note the differences in the cyclic voltammogram in 6 M CF_3SO_3H relative to the one obtained in a 1 M solution. In 6 M, the onset of the anodic oxide formation does not start until well beyond 0.9 V and is also less pronounced in the potential window below 1.2 V relative to a Pt/C in 1 M CF_3SO_3H. The onset of the anodic oxide film is directly related to the amount of free water available in the acid electrolyte; hence, the shift in the onset of the oxide formation in 6 M CF_3SO_3H at a potential beyond 0.9 V compared to that of 1 M CF_3SO_3H can be rationalized on the basis of the lower activity of water in high concentrations of the acid. As mentioned in the Experimental Section, since the reference electrodes were made from the same concentration of electrolyte as used in the experiments [hereafter referred to as RHE1 and RHE6 for hydrogen electrodes made from 1 and 6 M electrolytes, respectively], measured potentials at the working electrode are corrected for any Nernst shifts due to change in concentration of the electrolyte and all the voltammograms recorded are a direct reflection of the effect of water activation. In 6 M CF_3SO_3H solution, the number of free water molecules available would be less as a result of protonation of most of the free water molecules by CF_3SO_3H molecules. The number of water molecules associated with a molecule of CF_3SO_3H in a 6 M solution is only ∼4(mole ratio) as compared to 1 M CF_3SO_3H (∼50). Consequently, the activity of water is low in a 6 M solution and hence the shift in the formation of an anodic oxide, on the electrode and also the cathodic reduction currents of the oxide layer at about 0.8 V. The hydrogen adsorption desorption features are poorly resolved in a 6 M CF_3SO_3H compared to a 1 M CF_3SO_3H probably due to more pronounced mass transport effect in the electrolyte as also shown by others. The issue of any poisoning of the Pt surface due to impurities in the electrolyte or due to any kind of anion adsorption effects would

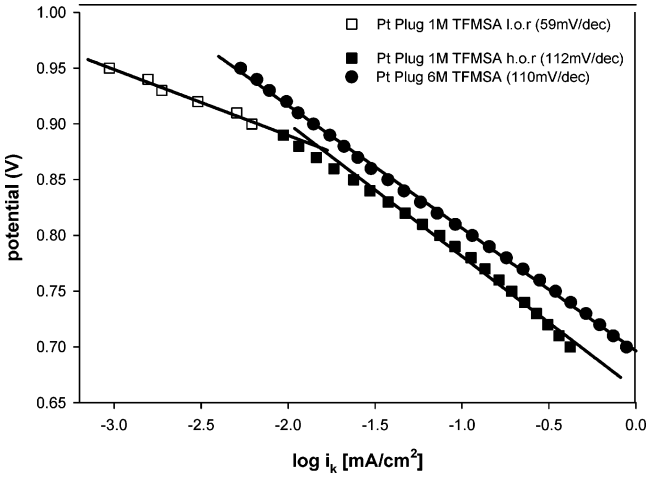

Figure 3. Tafel plots for ORR at room temperature on a polycrystalline (pc) Pt bulk electrode at 1225 rpm based on cathodic sweep from 1.2 V to 0.3 V at 25 mV/s in 1 and 6 M CF_3SO_3H.

be detrimental for ORR in high concentrations of the acid and would lead to a reduced activity of the Pt. However, the improved ORR activity on Pt/C in a 6 M TFMSA as would be shown in the next section suggests that the impurity effects from the acid can be neglected. A simple comparison of Figure 2a and Figure 2b suggests that the onset of an anodic oxide layer on Pt arising due to the oxidation of water molecules can be shifted by either alloying the Pt with metals that increase the 5*d*-band vacancies or by lowering the activity of water.

Oxygen Reduction Kinetics. Figure 3 shows the mass transport corrected Tafel plots obtained for a 6 mm diameter polycrystalline pc-Pt disk electrode on which oxygen reduction kinetics studies were conducted as a control experiment in 1 and 6 M CF_3SO_3H. The Tafel plots are obtained after the measured currents are corrected for diffusion to give the kinetic currents. Assuming a first-order reaction[57,79] for oxygen reduction, the kinetic current in the mixed activation−diffusion region is calculated from the equation

$$i_k = i_{lim} * i/(i_{lim} - i) \quad (1)$$

where i_k is the kinetic current density, i is the measured current density during the oxygen reduction polarization, and i_{lim} is the diffusion-limited current density, also known as the Levich current density. In the absence of a Nafion layer on the electrode, the limiting current density i_{lim} on the rotating disk electrode obeys the Levich equation

$$i_{lim} = B\omega^{1/2} \quad (2)$$

where ω is the rotation rate, and B is the Levich constant which is given as

$$B = 0.62 n_e F D^{2/3} \nu^{-1/6} C_o \quad (3)$$

where n_e is the number of electrons transferred per oxygen molecule during reduction, D is the diffusion coefficient of O_2 in the electrolyte, C_o is the O_2 concentration in the solution, and ν is the kinematic viscosity. In the case of a Nafion film-coated electrode, i_{lim} is dependent on the limiting current on the bare electrode and the diffusion through the Nafion film, assuming a steady-state concentration of oxygen at the electrolyte−film interface, this is expressed as

$$1/i_{lim} = 1/i_d + 1/i_f \quad (4)$$

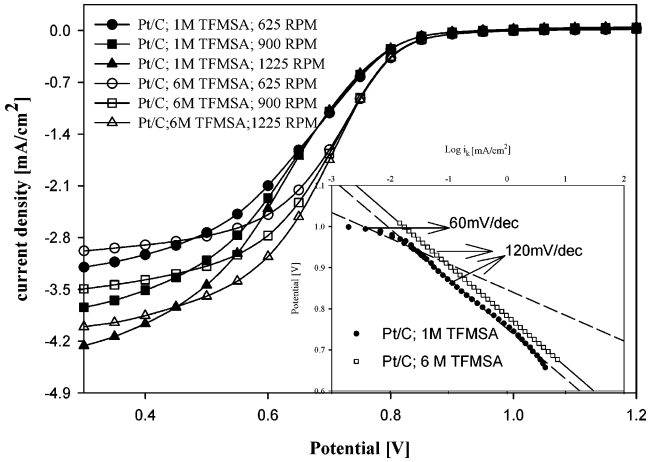

Figure 4. Disk currents obtained on the 20% Pt/C during ORR in the cathodic sweep at room temperature in 1 and 6 M CF_3SO_3H at various rotation rates (625, 900, and 1225 rpm). Inset shows the Tafel plots for ORR at room temperature at 1225 rpm based on cathodic sweep from 1.2 V to 0.3 V at 25 mV/s in 1 and 6 M CF_3SO_3H.

where i_d is the diffusion-limited current on the bare electrode, and i_f is the limiting current controlled by the transport of the reactant through the film and is given by the equation

$$i_f = n_e F D_f C_f / \delta_f \quad (5)$$

In this equation, D_f, C_f, and δ_f are the diffusion coefficient of O_2, concentration of O_2, and thickness of the Nafion film, respectively. The effect of the film diffusion is significant only in the case of an electrode covered by a Nafion film[22] and can be neglected in the present study since the amount of Nafion (20 μL in 5 mL of solution) in the prepared catalyst suspension is sufficiently small and hence not expected to be a factor in the limiting current density on the rotating electrode where only 20 μL of catalyst ink is loaded, resulting in 14 μg/cm^2 of catalyst and 0.08 μL of Nafion. The oxygen reduction reaction current can be written as dependent on the kinetic current and the diffusion-limited current as shown in eq 6:

$$1/i = 1/i_{lim} + 1/i_k = 1/B\omega^{1/2} + 1/i_k \quad (6)$$

In 1 M CF_3SO_3H, two Tafel slopes of 60 mV/decade at low current density and 120 mV/decade at high current density are observed (Figure 3) on a pc-Pt plug. The transition from 60 mV/decade to 120 mV/decade is closely related to the adsorbed OH species on Pt at potentials beyond 0.8 V vs RHE. A Tafel slope of $-2RT/F$, i.e., 120 mV/decade in the high overpotential region (h.o.r) is indicative of a surface that is clean hence devoid of any species that can affect the adsorption of O_2 from the solution to the active surface for reduction. However, in 6 M CF_3SO_3H, a single Tafel slope of 120 mV/decade was obtained in the entire potential range which is indicative of a clean active surface for oxygen reduction due to the lowering of water activation and hence lowering the poisoning effects of OH_{ads}.

Figure 4 shows the current density vs potential curves at different rotation rates (625, 900, 1225 rpm) for a carbon (Vulcan XC-72R) supported Pt in 1 and 6 M CF_3SO_3H at room temperature. The oxygen reduction is under a mixed kinetic and diffusion control in the potential range 0.9 and 0.6 V followed by a purely diffusion-limited region. The lower diffusion-limiting currents in 6 M CF_3SO_3H as compared to 1 M CF_3SO_3H can be explained on the basis of differences in diffusion coefficient and solubility of oxygen in these solutions. The diffusion coefficient and solubility of oxygen in these electro-

TABLE 3: Mass Transport Parameters (diffusion coefficient and concentration) of Oxygen in Different Electrolytes Determined Using Microelectrode Technique

electrolyte	$C \times 10^6$ (mol/cm^3)	$D \times 10^6$ (cm^2/s)	$DC \times 10^{12}$ (mol./cm s)	$D^{2/3}C \times 10^{10}$ (cm^2/s)$^{2/3}$ × (mol/cm^3)	$\nu^a \times 10^2$ (cm^2/s)
1 M CF_3SO_3H (25 °C)	0.63	9.67	6.09	2.86	0.917
6 M CF_3SO_3H (25 °C)	6.88	0.29	2.00	3.01	2.12
CF_3SO_3H[b] (25 °C)	1.6	9.5	15.2	7.17	
Nafion 117 (30 °C)	10.65	0.75	7.96		
Nafion 117[c] (30 °C)	9.34	0.995	9.3		
H_2SO_4[b] (25 °C)	1.1	14	15.4	6.4	
$HClO_4$[d]	1.18	19	22.42	8.4	0.893[d]

[a] Kinematic viscosity (viscosity/density). [b] From ref 89 Concentration of acid given as pH = 0. [c] From ref 90. [d] From ref 91 in low concentrated electrolytes.

lytes were measured using a micro electrode technique as described elsewhere[80] and are given in Table 3 along with the values found in the literature for CF_3SO_3H. In a rotating disk electrode experiment the permeability of oxygen to the electrode surface at a given rotation rate is dependent on $D^{2/3}\nu^{-1/6}C_o$ term in the Levich constant (B in eq 3) and differences in the diffusion coefficient, concentration of oxygen, and kinematic viscosity between 1 and 6 M TFMSA are directly reflected in the diffusion-limiting currents obtained in these electrolyte concentrations. Although the concentration of oxygen in 6 M CF_3SO_3H is significantly higher than that of 1 M electrolyte (Table 3), the diffusion coefficient shows quite an opposite trend and the product of D and C are very similar for 1 and 6 M TFMSA. However, incorporating the kinematic viscosity (shown in Table 3) into the Levich equation, the diffusion-limited currents follows the same trend as the overall permeability of oxygen ($D^{2/3}\nu^{-1/6}C_o$) to the electrode surface in these electrolytes to a good approximation.

It can be seen from Figure 4 that the rate of increase in cathodic currents due to ORR in 6 M CF_3SO_3H is faster than that in 1 M CF_3SO_3H, even though the limiting current density is lower as mentioned above due to oxygen permeability in these electrolytes. In the mixed potential range between 0.9 and 0.6 V, at a given current density, Pt/C in 6 M CF_3SO_3H exhibits ~40 mV lower overpotential than Pt/C in 1 M CF_3SO_3H. This can be correlated to the number of Pt sites that are covered by surface adsorbed −OH species which are greatly reduced in 6 M acid concentration. The inset in Figure 4 shows the mass transport corrected Tafel slopes obtained for the Pt/C in 1 and 6 M CF_3SO_3H. It can be seen that a Pt/C exhibits the same Tafel behavior as a bulk polycrystalline pc-Pt in both 1 and 6 M TFMSA. A single slope of 120 mV/decade in 6 M TFMSA is indicative of a clean active surface of Pt for the reduction of oxygen and a lowering in the overpotential by about 40 mV is a direct consequence of inhibition of OH_{ads} on the surface due to the lower activity of water in 6 M CF_3SO_3H.

The current density vs potential curves for oxygen reduction on PtCo/C and PtFe/C in 1 and 6 M CF_3SO_3H measured at various rotation speeds are shown in Figures 5 and 6, respectively. The kinetic data for all the electrocatalysts are compared and summarized in Table 4. Compared to the Pt/C in 1 M TFMSA, the 1 M data for PtCo/C and PtFe/C show significantly improved kinetic currents for ORR. The kinetic currents follow the trend Pt/C < PtFe/C < PtCo/C (Table 4). All the kinetic currents are based on a metal geometric loading of 14 μg/cm^2. The kinetic currents for PtFe/C and PtCo/C alloys would show a much higher improvement when compared on the basis of electrochemically active surface areas (Table 4) of Pt. However, in 6 M CF_3SO_3H, the Pt−M/C (M = Fe and Co) alloys do not show the same trend in their kinetic currents compared to Pt/C. The activity of Pt/C is higher than that of the Pt−M/C alloys

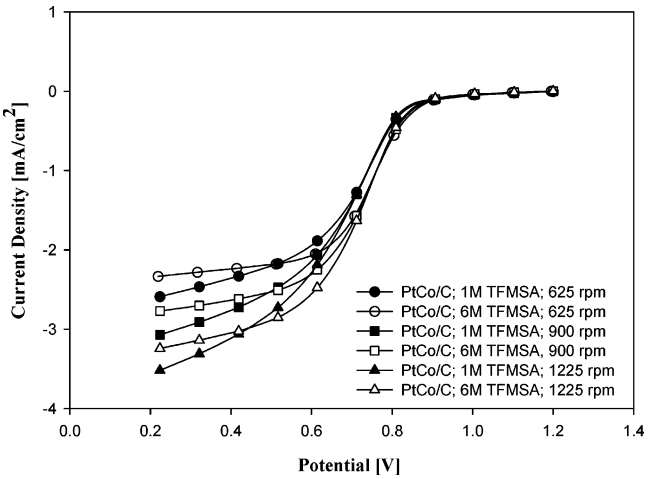

Figure 5. Disk currents obtained on the PtCo/C during ORR in the cathodic sweep at room temperature in 1 and 6 M CF_3SO_3H at various rotation rates (625, 900, and 1225 rpm) measured at room temperature.

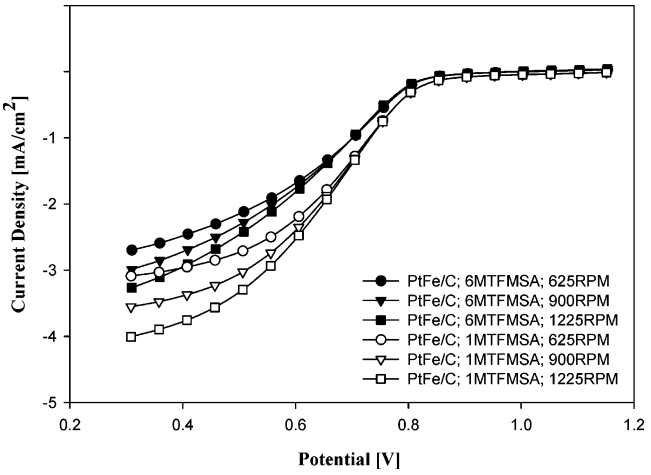

Figure 6. Disk currents obtained on the PtFe/C during ORR in the cathodic sweep at room temperature in 1 and 6 M CF_3SO_3H at various rotation rates (625, 900, and 1225 rpm) measured at room temperature.

for ORR in 6 M TFMSA in contrast to that observed in 1 M concentration. This implies that although a change in Pt d-band vacancies in Pt−M alloys improves their oxygen reduction kinetics in a fully hydrated environment (1 M concentration) by lowering the anodic oxidation of water, it fails to explain the improved kinetics for a Pt/C in 6 M TFMSA. Hence a strategy to enable lower water activation without significantly affecting the d-band vacancy appears to be the best option. In summary, Figures 7 and 8 show the comparison of the supported Pt with PtFe/C and PtCo/C in 1 and 6 M CF_3SO_3H at a rotation rate of 1225 rpm, respectively. In 1 M CF_3SO_3H (Figure 7),

TABLE 4: Electrode Kinetic Parameters for the Different Electrocatalysts in 1 and 6 M CF_3SO_3H (TFMSA) at Room Temperature from RRDE Experiments at 1225 rpm

catalyst	concn. of TFMSA	I_k 0.9 V (mA/cm^2)	I_k 0.8 V (mA/cm^2)	$-\log I_0$ (mA/cm^2)	Tafel slope (mV/decade)	active surface area[a] [charge H_{upd} region from CV in 1 M TFMSA] (cm^2)
pc-Pt plug	1 M	0.006	0.074	7.64/4.77	59/113	0.504
	6 M	0.014	0.114	4.85	110	
20%Pt/C	1 M	0.057	0.426	6.19/3.95	60/119	2.103
	6 M	0.122	0.607	3.65	123	
20%PtCo/C	1 M	0.106	0.413	3.39	140	1.177
	6 M	0.101	0.458	3.35	142	
20%PtFe/C	1 M	0.085	0.389	3.30	146	1.662
	6 M	0.033	0.245	4.40	113	

[a] Based on 210 $\mu C/cm^2$ for atomic hydrogen oxidation on a smooth Pt surface.

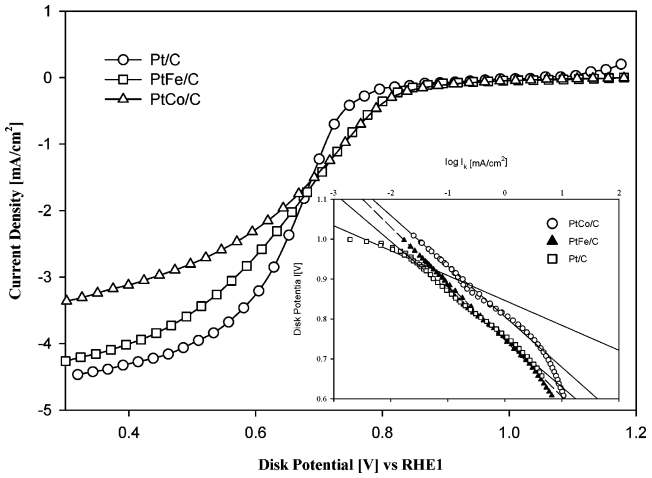

Figure 7. Disk currents obtained on Pt/C, PtCo/C, and PtFe/C during ORR in the cathodic sweep at room temperature in 1 M CF_3SO_3H at 1225 rpm at 25 mV/s at room temperature. Inset. Tafel plots for Pt/C (□), PtCo/C (○), and PtFe/C(▲); rotation rate, 1225 rpm.

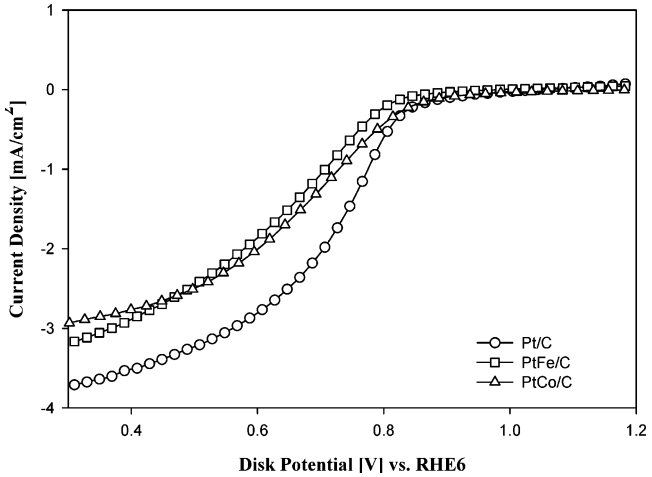

Figure 8. Disk currents obtained on Pt/C, PtCo/C, and PtFe/C during ORR in the cathodic sweep at room temperature in 6 M CF_3SO_3H at 1225 rpm at 25 mV/s at room temperature.

the supported PtM alloys show improved oxygen reduction kinetics than Pt/C above 0.8 V. This enhanced ORR kinetics is an indication of the shift in the formation of an oxide layer on Pt, facilitated by alloying with transition metals which increase the *d*-band character of Pt. This is also reflected in a single Tafel slope of 120 mV/decade observed in the PtM alloy catalysts (inset in Figure 7), whereas Pt/C shows two slopes of 60 and 120 mV/decade (inset in Figure 4). However, comparing the three electrocatalysts in 6 M CF_3SO_3H (Figure 8) shows a

TABLE 5: Activation Energies for Oxygen Reduction for the Different Electrocatalysts in 1 M CF_3SO_3H as a Function of Electrode Potential

electro-catalyst	E_a* (0.85V) (kJ/mol)	E_a* (0.80V) (kJ/mol)	E_a* (0.75V) (kJ/mol)	E_a* (0.70V) (kJ/mol)
Pt/C	27.84 ± 2.04	26.87 ± 2.0	22.13 ± 1.7	19.12 ± 1.8
PtCo/C	27.86 ± 0.23	25.18 ± 0.78	22.33 ± 0.33	19.02 ± 0.78
PtFe/C	19.3	19.4	18.66	17.55

complete reversal of oxygen reduction kinetics following the trend PtFe/C < PtCo/C < Pt/C. Although the results discussed so far indicate that alloying Pt with transition metals and altering its *d*-band character does not improve its activity for oxygen reduction kinetics at low water content, the alloy electrocatalysts have more implications on the stability of catalysts in terms of its effect on their oxygen reduction reaction pathways which is an important factor to consider toward the stability of the polymer electrolyte−electrode interface

The activation energies for oxygen reduction reaction for the various electrocatalysts were evaluated at a fixed electrode potential based on a modified Arrhenius equation as shown below:

$$\left(\frac{\partial \log(i_k)}{\partial(1/T)}\right)_E = \frac{E_a^*}{2.3R} \tag{7}$$

The procedure for calculating the activation energies at different electrode potentials followed the steps described in detail elsewhere.[61,65]

The activation energies determined in 1 M CF_3SO_3H using a linear regression analysis for the three different electrocatalysts are shown in Table 5. The data shows that within the limits of error, there is very little difference between the activation energies of Pt and PtCo alloy electrocatalysts. PtFe/C does show a smaller value which follows a similar trend with change in electrode potentials as Pt/C and PtCo/C. The reason for this consistently lower value is not well understood. Such a similarity in activation energy between Pt/C and PtCo/C alloy electrocatalysts is in close agreement with a previously published report by Paulus et al.[65] where three different electrocatalysts Pt/C, PtCo/C, and PtNi/C were examined in 0.1 M $HClO_4$ using a similar RRDE technique. The activation energies reported at three different overpotentials (0.3, 0.35, and 0.4 V) with respect to the theoretical reversible potential for oxygen reduction of 1.23 V were in very close agreement with those found in our work. However, in their report, no trend with respect to overpotential was discerned. Our results show a trend with respect to overpotential (electrode potential varied between 0.9 and 0.7 V) vs RHE. The implication of this trend is complicated and will be discussed in a later publication.[81] However, the close values of activation energies between Pt and Pt alloys in 1 M

TFMSA clearly indicate that the differences in oxide layer formation on Pt alloys as compared to Pt is primarily linked to the preexponential term in the Arrhenius rate expression. This can be explained on the basis of a conventional rate expression as shown in eq 8 which involves using transition states and their surface coverage as determined by Markovic et al.[65,82] assuming that the first electron transfer for oxygen reduction is the rate-determining step:

$$i = nFkC_o(1 - \Theta_{ads}) \exp(-\beta FE/RT) \exp(-\gamma r\Theta_{ads}/RT) \quad (8)$$

where E is the applied potential, i is the observed current density, n is the number of electrons, k is the rate constant, C_o is the concentration of oxygen, Θ_{ads} is the surface coverage of adsorbed intermediates, and β and γ are the symmetry factors. Here, the term $r\Theta_{ads}$ was related to the apparent Gibbs energy of adsorption associated with surface coverage of an oxide layer. The close values of the activation energies observed for all the three electrocatalyst also suggests that the transition state in the activation energy profile therefore remains unchanged. Anderson et al.[83−85] have previously shown that the activation energy for ORR decreased with an increase in overpotential which is consistent with the observed activation energies in this work for all the three electrocatalysts. The ab initio calculations[85] for a series of four one-electron oxygen reduction reactions based on electronic equilibrium of the transition state complex with the electrode potential predicted that the activation energies for all four steps decreased with an increase in overpotential with the H_2O_2 (intermediate) reduction having the highest activation energy followed by the first electron reduction of oxygen. The reduction of ·OOH and ·OH intermediates were calculated to have the lowest activation energies. The decrease in activation energies with increasing overpotential found experimentally in this study is in close agreement with the activation energies found theoretically and follows the same trend as predicted by the theory.

Oxygen Reduction Pathway on Pt/C and Pt Alloys. The reaction pathway for oxygen reduction reaction for the formation of relative amounts of H_2O_2 and H_2O can be determined quantitatively with an RRDE experiment by holding the potential of the ring at a constant potential of 1.2 V where the H_2O_2 formed on the disk during oxygen reduction is readily oxidized. Figure 9a shows the currents (I_R) obtained on a gold ring electrode during oxygen reduction on Pt/C in 1 and 6 M CF_3SO_3H at 1225 rpm. The ring currents are negligible in the potential region above 0.6 V in 1 M CF_3SO_3H, indicating that the reduction of oxygen proceeds almost completely by a four-electron transfer above this potential which is relevant for the operating potential of fuel cell cathodes. However, the ring currents in 6 M CF_3SO_3H, although relatively very small compared to four-electron ORR, shows ∼ 4-fold enhancement compared to 1 M CF_3SO_3H. This is very significant with regard to choice of polymer electrolyte membranes in fuel cells where H_2O_2 is a potential source of degradation of membranes with prolonged exposure. Especially for nonfluorinated membranes currently being considered as potential replacement for Nafion-type polymer electrolytes in a quest for elevated (up to 130 °C) temperature operation. Most of these membranes are based on engineered polymers with high thermo-chemical stability,[86] typically with a high degree of aromatic character, where the monomer consists of a variety of fused phenyl rings linked together with a number of bridging aromatic backbones and consisting of sulfonic acid-substituted aromatic rings. Of the two degradation mechanisms postulated for nonfluorinated membranes during the long-term fuel cell operations, (1) oxygen diffusing through the membrane to the anode where the HOO• radicals formed at the surface of the catalyst attacks the tertiary hydrogen at the α-carbon of the polymer;[87,88] (2) oxygen reduction at the cathode proceeding through a peroxide intermediate (H_2O_2), which reacts with trace metal ions in the membrane to form HOO• and HO• radicals, which in turn results in membrane degradation at cathode during oxygen reduction reaction,[43] the latter is directly linked to cathode electrode electrocatalysis.

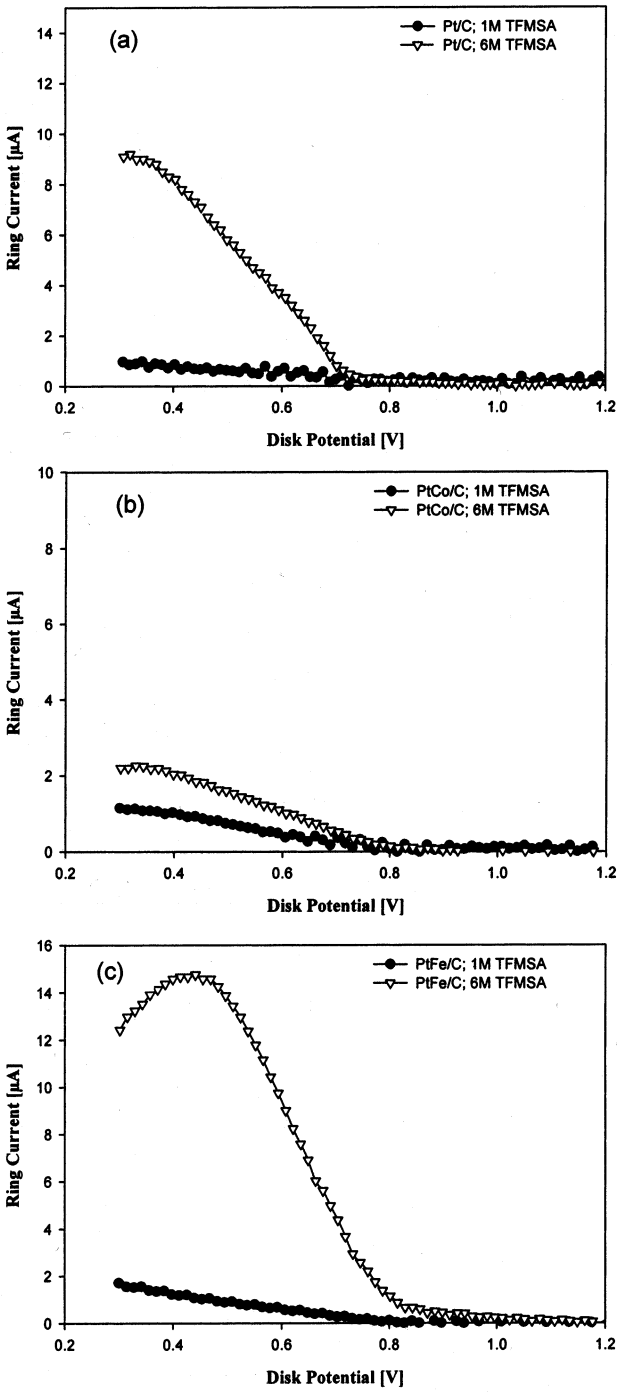

Figure 9. (a) Ring currents obtained on Pt/C during ORR in the cathodic sweep at room temperature in 1 and 6 M CF_3SO_3H at 1225 rpm at room temperature. (b) Ring currents obtained on PtCo/C during ORR in the cathodic sweep at room temperature in 1 and 6 M CF_3SO_3H at 1225 rpm in room temperature. (c) Ring currents obtained on PtFe/C during ORR in the cathodic sweep at room temperature in 1 and 6 M CF_3SO_3H at 1225 rpm in room temperature.

TABLE 6: Comparison of Mole Fraction of Peroxide Formed for the Pt and Pt Alloy Catalysts at 0.7 and 0.6 V from RRDE Experiments at 1225 rpm, Room Temperature

catalyst	$\%H_2O_2$, 1 M TFMSA [@0.7 V]	$\%H_2O_2$, 6 M TFMSA [@0.7 V]
Pt/C	0.114	0.416
PtFe/C	0.147	2.387
PtCo/C	0.151	0.301

TABLE 7: Ring Currents Obtained at 0.7 and 0.6 V during Oxygen Reduction Reaction on Pt/C and PtM/C (M = Fe and Co) Catalysts during Cathodic Sweep between 1.2 V and 0.3 V at Room Temperature

catalyst	concn. of TFMSA	$I_r[\mu A]$ 0.7 V	$I_r[\mu A]$ 0.6 V
Pt/C	1 M	0.27	0.49
	6 M	0.90	3.60
PtFe/C	1 M	0.33	0.67
	6 M	4.43	9.37
PtCo/C	1 M	0.30	0.53
	6 M	0.54	1.01

Table 6 shows the relative amounts of H_2O_2 (% H_2O_2 formed compared to ORR) formed on the electrocatalyts in 1 and 6 M CF_3SO_3H based on the equation

$$\chi_{H_2O_2} = \frac{2I_R/N}{I_D + I_R/N} \qquad (9)$$

$$N^* = 0.2$$

where N is the collection efficiency of the ring, χ is the mole fraction of peroxide formed, I_D and I_R are the disk and ring currents, taking into account the total disk currents for the oxygen reduction as the sum of reduction currents of O_2 to H_2O and H_2O_2 and the collection efficiency N for the ring electrode.[61] At the typical operating potentials of a fuel cell 0.7 V, H_2O_2 formation at steady state is ~0.11% in 1 M CF_3SO_3H and ~0.42% in 6 M CF_3SO_3H on a 20% Pt/C electrode. However, the amounts of peroxides formed on supported Pt alloys (PtCo/C and PtFe/C) are very different. The amounts of peroxides formed on a PtCo/C in 1 and 6 M CF_3SO_3H show almost the same trend as the Pt/C, however the ring current detected in 6 M TFMSA is significantly lower than that of Pt/C (Figure 9b). Also the ORR kinetic currents on PtCo/C did not show any dramatic enhancement between 1 and 6 M CF_3SO_3H, whereas the Pt/C showed a significant increase in the kinetic currents due to oxygen reduction in 6 M CF_3SO_3H. This suggests that the oxygen reduction may have a small but negligible peroxide formation step on Pt/C. This tends to agree with a simultaneous mechanism as suggested by Damjanovic et al.[13] where some small part of the oxygen reduction reaction goes through a peroxide intermediate. However, the peroxide formation on a PtFe/C showed a contrasting behavior. The considerable decrease in the ORR kinetic currents for PtFe/C (Figure 6) in 6 M CF_3SO_3H compared to that in 1 M CF_3SO_3H would be expected to generate lower peroxide currents at the ring if it were to follow the previous trend. In contrast to PtCo/C, PtFe/C shows a large increase in peroxide yield at 6 M concentration. This shows that choice of alloy element has a significant effect on parallel pathway for ORR where activity of water is low. Further, peroxide currents exhibit a greater increase with decrease in potentials for PtFe/C in 6 M concentration as compared to Pt/C and PtCo/C (Table 7). Since we started with a PtFe/C with predominantly a Pt skin,[2,77] and the increase in the peroxide current on a PtFe/C in 6 M CF_3SO_3H suggests the possibility of Fe atoms on the electrocatalyst surface, further surface studies in high concentrations of TFMSA are needed to get a better understanding of the electrocatalytic activity of these Pt-M/C (M = transition metal) alloys.

Conclusions

From the results discussed above it is evident that the oxygen reduction reaction on an electrocatalyst surface depends on the nature of Pt surface (alloyed or unalloyed) as determined by the surface electronic properties which affects water activation in a fully hydrated state. Alloying Pt with transition metals such as Co and Fe followed by a washing step in 1 M $HClO_4$ (24 to 48 h) enables an alloy inner core with an outer layer rendered predominantly Pt. The consequence of such alloy nanoparticle formation is a significant lowering of water activation beyond 0.8 V vs RHE, in contrast to Pt/C.

The lower affinity toward water activation in a fully hydrated environment (1 M TFMSA) for Pt alloys in contrast to Pt is manifested in the observed Tafel slope which is 120 mV/decade ($2RT/F$) for the alloys in contrast to the expected value of 60 mV/decade, observed on both pc-Pt and Pt/C. Such a lowering of affinity toward water activation on Pt alloys in 1 M concentration is also reported using cyclic voltammograms as well as in-situ XAS data. Both the in-situ XANES and EXAFS data analysis comparing Pt L_3 edge spectra at 0.54 and 0.84 V vs RHE for alloys clearly indicate lack of any oxide coverage. This is in contrast to Pt/C where, as expected, an increase in white line intensity (directly related to Pt *d*-band vacancy) is observed at 0.84 V relative to 0.54 V due to formation of Pt oxides. Comparison of Pt L_3 edge EXAFS data confirms this and provides an alternative probe of this phenomenon.

Such a lowering of affinity of oxide formation, a surface poison for molecular oxygen adsorption on Pt alloys in the fully hydrated analogue (1 M TFMSA) is correlated to a concomitant increase in ORR activity as shown by RDE data. However, a lowering of water activity resulting from a shift in concentration to 6 M shows that while there is an increase in ORR activity for Pt/C due to lowering of surface oxide formation, a corresponding effect with Pt alloys does not occur. This further supports our earlier contention of ORR activity being dependent on surface coverage by oxides. Further, a more important conclusion from the lack of increased activity for Pt alloys in 6 M concentration of TFMSA is that the process of alloying with transition metals does not render the surface of the catalyst to be inherently more active for oxygen reduction, in contrast to the increased activity observed for the alloys in 1 M concentration. This is related to a wealth of prior literature as discussed in our Results and Discussion section where the rate-limiting step for oxygen reduction reaction in a fully hydrated state (1 M concentration) is the initial dissociative adsorption of molecular oxygen. Significant changes to the electronic states of Pt as a consequence of alloying could affect the affinity for molecular oxygen adsorption. This is a strong possibility supported by our data in 6 M TMFSA; its confirmation is a subject of theoretical simulations, which are currently being conducted by us.

Measured activation energies at 1 M concentration show very close values between Pt/C and PtCo/C with PtFe/C somewhat lower. These activation energies also exhibited a common trend wherein a lowering was observed with increase in overpotential. The relatively similar values of activation energy for Pt and Pt alloys seem to indicate that the differences in ORR activity arises primarily from contributions to the preexponential term in the Arrhenius expression, of which the prime contributor is the surface coverage of oxides. The similar trend of changes in

activation energy values with electrode potential requires more theoretical insight which will be the subject of a separate manuscript.

The issue of relative yield of peroxides on the Pt and Pt alloy surface in 1 and 6 M TFMSA shows interesting variations. Peroxide yield albeit small (less than one percent of four-electron oxygen reduction) was observed below 0.6V vs RHE in both 1 and 6 M TFMSA, exhibiting an exponential rise with overpotential. However, comparison of Pt and Pt alloys at 1 M concentration in the potential region below 0.6 V shows that peroxide yield is similar on all the electrocatalysts. Transition to 6 M concentration however causes a much bigger enhancement in peroxide yield for PtFe/C followed by Pt/C and was least for PtCo/C. This sensitivity of peroxide yield with choice of electrocatalyst has the potential of major impact on interfacial stability, especially for non fluorinated membranes operating at elevated temperature under less than 100% relative humidity conditions.

Overall, the observation of lower inherent activity for molecular oxygen reduction in Pt alloy electrocatalysts when the issue of water activation is removed as an influence (such as higher concentration acid environment without concomitant poisoning with anionic species, etc.) has the potential for a major impact in our choice of alloying elements. Much more work needs to be done for enabling better tuning of the Pt electronic states (which are responsible for controlling the affinity for water activation and adsorption of molecular oxygen) by processes such as alloying (in this case) and others such as introduction of metal polymer interactions.

Acknowledgment. The authors gratefully acknowledge the financial support from the Army Research Office. One of the authors (R.C.U.) thanks the U. S. Department of Education for its support of the GANN Fellowship. The help rendered by Lei Zhang, Northeastern University, to determine the diffusion coefficient and concentration of oxygen in the electrolytes is deeply appreciated. The authors also thank Dr. M. A. Enayetullah, Protonex Technology Corp., for valuable advice and discussions regarding the safe handling and distillation of trifluoromethane sulfonic acid.

References and Notes

(1) Mukerjee, S.; Srinivasan, S. *J. Electroanal. Chem.* **1993**, *357*, 201.
(2) Mukerjee, S.; Srinivasan, S.; Soriaga, M. P. *J. Electrochem. Soc.* **1995**, *142*, 1409.
(3) Mukerjee, S.; Srinivasan, S.; Soriaga, M. P.; McBreen, J. *J. Phys. Chem.* **1995**, *99*, 4577.
(4) Tamizhmani, G.; Capuano, G. A. *J. Electrochem. Soc.* **1994**, *141*, 968.
(5) Friedrich, K. A.; Beck, T.; Garche, J.; Stimming, U. *Abstracts of Papers, 223rd ACS National Meeting, Orlando, FL, United States, April 7−11, 2002* **2002**, COLL.
(6) Kalhammer, F. R.; Prokopius, P. R.; Roan, V. R.; Voecks, G. E. In "*Status and Prospects of Fuel Cells as Automotive Engines*"; Air Resources Board, California Environmental Agency; July, 1998.
(7) Srinivasan, S. *J. Electrochem. Soc.* **1989**, *136*, 41C.
(8) Appleby, A. J.; Foulkes, F. R. *Fuel Cell Handbook*; van Nostrand Reinhold: New York, 1989.
(9) Wroblowa, H.; Rao, M. L. B.; Damjanovic, A.; Bockris, J. O. M. *J. Electroanal. Chem. Interfacial Electrochem.* **1967**, *15*, 139.
(10) Bockris, J. O. M.; Srinivasan, S. Fuel Cells: Their Electrochemistry; McGraw-Hill: New York, 1969; p 469.
(11) Mukerjee, S. In Situ X-ray Absorption of Carbon-Supported Pt and Pt Alloy Electrocatalysts: Correlation of Electrocatalytic Activity with Particle Size and Alloying. In *Catalysis and Electrocatalysis at Nanoparticle Surfaces*; Wieckowski, A., Savinova, E. R., Vayenas, C. G., Eds.; Marcel Dekker: New York, 2003.
(12) Adzic, R. R. In *Electrocatalysis*; Lipkowski, J., Ross, P. N., Eds.; Wiley-VCH: New York, 1998; p 197.
(13) Damjanovic, A.; Brusic, V.; Bockris, J. O. M. *J. Phys. Chem.* **1967**, *71*, 2741.
(14) Yeager, E.; Razaq, M.; Gervasio, D.; Razaq, A.; Tryk, D. *Proc. Electrochem. Soc.* **1992**, *92−11*, 440.
(15) Yeager, E.; Razaq, M.; Gervasio, D.; Razaq, A.; Tryk, D. *J. Serb. Chem. Soc.* **1992**, *57*, 819.
(16) Clouser, S. J.; Huang, J. C.; Yeager, E. *J. Appl. Electrochem.* **1993**, *23*, 597.
(17) Yeager, E. Electrocatalysts for oxygen electrodes: final report; Department of Chemistry, Case Western Reserve University, Cleveland, OH. FIELD URL:, 1990.
(18) Yeager, E. *Electrochim. Acta* **1984**, *29*, 1527.
(19) Tarasevich, M. R.; Vilinskaya, V. S. *Electrokhimiya* **1973**, *9*, 96.
(20) Adzic, R. R. In *Structural Effects in Electrocatalysis and Oxygen Electrochemistry, Proceedings Vol. 92−11*; Scherson, D. D., Tryk, D., Daroux, M., Xing, X., Eds.; The Electrochemical Society: Pennington, NJ, 1992; p 419.
(21) Uribe, F. A.; Springer, T. E.; Wilson, M. S.; Zawodzinski, T. A., Jr.; Gottesfeld, S. *Proc. Electrochem. Soc.* **1996**, *95* (26), 50.
(22) Markovic, N. M.; Gasteiger, H. A.; Ross, P. N., Jr. *J. Phys. Chem.* **1995**, *99*, 3411.
(23) Faguy, P. W.; Marinkovic, N. S.; Adzic, R. R. *Langmuir* **1996**, *12*, 243.
(24) Mukerjee, S.; McBreen, J. *Proc. Electrochem. Soc.* **1996**, *96* (8), 421.
(25) McBreen, J.; Mukerjee, S. *J. Electrochem. Soc.* **1995**, *142*, 3399.
(26) Jalan, V.; Taylor, E. J. *J. Electrochem. Soc.* **1983**, *130*, 2299.
(27) Paffett, M. T.; Beery, J. G.; Gottesfeld, S. *J. Electrochem. Soc.* **1988**, *135*, 1431.
(28) Kinoshita, K. *J. Electrochem. Soc.* **1990**, *137*, 845.
(29) Beard, B. C.; Ross, P. N. *J. Electrochem. Soc.* **1990**, *130*, 3368.
(30) Mukerjee, S. *J. Appl. Electrochem.* **1990**, *20*, 537.
(31) Conway, B. E.; Novak, D. M. *J. Electrochem. Soc.* **1981**, *128*, 956.
(32) Mukerjee, S.; McBreen, J.; Srinivasan, S. *Proc. Electrochem. Soc.* **1996**, *95* (26), 38.
(33) Habib, M. A.; Bockris, J. O. *J. Electrochem. Soc.* **1983**, *130*, 2510.
(34) Enayetullah, M. A.; DeVilbiss, T. D.; Bockris, J. O. M. *J. Electrochem. Soc.* **1989**, *136*, 3369.
(35) Zinola, C. F.; Triaca, W. E.; Arvia, A. J. *J. Appl. Electrochem.* **1995**, *25*, 740.
(36) Zinola, C. F.; Luna, A. M. C.; Triaca, W. E.; Arvia, A. J. *J. Appl. Electrochem.* **1994**, *24*, 119.
(37) Paulus, U. A.; Wokaun, A.; Scherer, G. G.; Schmidt, T. J.; Stamenkovic, V.; Markovic, N. M.; Ross, P. N. *Electrochim. Acta* **2002**, *47*, 3787.
(38) Zinola, C. F.; Luna, A. M. C.; Triaca, W. E.; Arvia, A. J. Electroreduction of molecular oxygen on preferentially oriented platinum electrodes in acid solution. In *J. Appl. Electrochem.* **1994**, *24*, 119.
(39) Zinola, C. F.; Triaca, W. E.; Arvia, A. J. Kinetics and mechanism of the oxygen electroreduction reaction on faceted platinum electrodes in trifluoromethanesulfonic acid solutions. In *J. Appl. Electrochem.* **1995**, *25*, 740.
(40) Paulus, U. A.; Wokaun, A.; Scherer, G. G.; Schmidt, T. J.; Stamenkovic, V.; Markovic, N. M.; Ross, P. N. Oxygen reduction on high surface area Pt-based alloy catalysts in comparison to well-defined smooth bulk alloy electrodes. *Electrochim. Acta* **2002**, *47*, 3787.
(41) Adzic, R. R. In *Electrocatalysis, Proc. Symp.*; O'Grady, W. E., Ross, P. N., Will, F. G., Eds,; The Electrochemical Society: Pennington, NJ, 1992; p 419.
(42) Anastasijevic, N. A.; Vesovic, V.; Adzic, R. R. *J. Electroanal. Chem. Interfacial Electrochem.* **1987**, *229*, 305.
(43) Guo, Q.; Pintauro, P. N.; Tang, H.; O'Connor, S. *J. Membrane Sci.* **1999**, *154*, 175.
(44) Kotz, R.; Clouser, S.; Sarangapani, S.; Yeager, E. *J. Electrochem. Soc.* **1984**, *131*, 1097.
(45) Habib, M. A.; Bockris, J. O. *Compr. Treatise Electrochem.* **1980**, *1*, 135.
(46) Hyde, P. J.; Maggiore, C. J.; Redondo, A.; Srinivasan, S.; Gottesfeld, S. *J. Electroanal. Chem. Interfacial Electrochem.* **1985**, *186*, 267.
(47) Enayetullah, M. A. Ph.D. Thesis. Case Western Reserve University, 1986.
(48) Conway, B. E.; Novak, D. M. Hysteresis in Formation and Reduction of Submonolayer Quantities of Surface Oxide at Pt in an Almost Anhydrous Solvent. In *J. Electrochem. Soc.* **1981**, *128*, 956.
(49) Enayetullah, M. A.; DeVilbiss, T. D.; Bockris, J. O. M. Activation parameters for oxygen reduction kinetics in trifluoromethanesulfonic acid systems. In *J. Electrochem. Soc.* **1989**, *136*, 3369.
(50) Jalan, V. M.; Bushnell, C. L. Highly dispersed catalytic platinum. In *U. S.; (United Technologies Corp., USA)*, 1979; 4 pp.
(51) Jalan, V. M. Cathode alloy electrocatalysts. In *Eur. Pat. Appl.*; Giner, Inc., USA, 1985; 10 pp.
(52) Landsman, D. A.; Luczak, F. J. Precious metal-chromium alloy catalyst for fuel cell electrodes. In *Belg.*; (United Technologies Corp., USA), 1981; 16 pp.

(53) Stonehart, P.; Watanabe, M.; Yamamoto, N.; Nakamura, T.; Hara, N.; Tsurumi, K. Platinum alloy electrode catalyst. In *Jpn. Kokai Tokkyo Koho*; (Stonehart Associates Inc., USA), 1992; 5 pp.
(54) Urian, R. C.; Murthi, V. S.; Mukerjee, S. In preparation.
(55) Gong, S.; Lu, J.; Yan, H. *J. Electroanal. Chem.* **1997**, *436*, 291.
(56) Will, F. G. *J. Electrochem. Soc.* **1986**, *133*, 454.
(57) Ross, P. N.; Andricacos, P. C. *J. Electroanal. Chem. Interfacial Electrochem.* **1983**, *154*, 205.
(58) Parthasarathy, A.; Brumlik, C. J.; Martin, C. R. *Polym. Mater. Sci. Eng.* **1993**, *68*, 117.
(59) Holdcroft, S.; Abdou, M. S.; Beattie, P.; Basura, V. *New Mater. Fuel Cell Mod. Battery Syst. II, Proc. Int. Symp., 2nd* **1997**, 861.
(60) Lee, H. S.; Yang, X.-o.; McBreen, J.; Xiang, C. Boron compounds as anion binding agents for nonaqueous battery electrolytes. In *U. S.*; (Brookhaven Science Associates, USA), 2000; 11 pp.
(61) Paulus, U. A.; Schmidt, T. J.; Gasteiger, H. A.; Behm, R. J. *J. Electroanal. Chem.* **2001**, *495*, 134.
(62) Gojkovic, S. L.; Zecevic, S. K.; Savinell, R. F. *J. Electrochem. Soc.* **1998**, *145*, 3713.
(63) Zecevic, S. K.; Wainright, J. S.; Litt, M. H.; Gojkovic, S. L.; Savinell, R. F. *J. Electrochem. Soc.* **1997**, *144*, 2973.
(64) Schmidt, T. J.; Paulus, U. A.; Gasteiger, H. A.; Alonso-Vante, N.; Behm, R. J. *J. Electrochem. Soc.* **2000**, *147*, 2620.
(65) Paulus, U. A.; Wokaun, A.; Scherer, G. G.; Schmidt, T. J.; Stamenkovic, V.; Radmilovic, V.; Markovic, N. M.; Ross, P. N. *J. Phys. Chem. B* **2002**, *106*, 4181.
(66) Wong, J.; Lytle, F. W.; Messmer, R. P.; Maylotte, D. H. *Phys. Rev. B: Condensed Matter and Materials Physics* **1984**, *30*, 5596.
(67) Mansour, A. N.; Cook, J. W., Jr.; Sayers, D. E.; Emrich, R. J.; Katzer, J. R. *J. Catalysis* **1984**, *89*, 462.
(68) Mansour, A. N.; Cook, J. W., Jr.; Sayers, D. E. *J. Phys. Chem.* **1984**, *88*, 2330.
(69) McBreen, J. *Phys. Electrochem.* **1995**, 339.
(70) Van Zon., J. B. A. D.; Koningsberger, D. C.; Van't Blik., H. F. J.; Sayers, D. E. *J. Chem. Phys.* **1985**, *82*, 5742.
(71) Duivenvoorden, F. B. M.; Koningsberger, D. C.; Uh, Y. S.; Gates, B. C. *J. Am. Chem. Soc.* **1986**, *108*, 6254.
(72) Mukerjee, S.; Urian, R. C. *Electrochim. Acta* **2002**, *47*, 3219.
(73) Uribe, F. A.; Springer, T. E.; Gottesfeld, S. *J. Electrochem. Soc.* **1992**, *139*, 765.
(74) Gonzalez, E. R.; Srinivasaan, S. *Electrochim. Acta* **1982**, *27*, 1425.
(75) Zelenay, P.; Habib, M. A.; Bockris, J. O. M. *J. Electrochem. Soc.* **1984**, *131*, 2464.
(76) Mukerjee, S.; Srinivasan, S.; Soriaga, M. P. Role of structural and electronic properties of Pt and Pt alloys on electrocatalysis of oxygen reduction. An in situ XANES and EXAFS investigation. In *J. Electrochem. Soc.* **1995**, *142*, 1409.
(77) Ruban, A. V.; Skriver, H. L.; Norskov, J. K. *Phys. Rev. B: Condensed Matter and Materials Physics* **1999**, *59*, 15990.
(78) Benfield, R. E. *J. Chem Soc., Faraday Trans.* **1992**, *88*, 1107.
(79) Ross, P. N.; Cairns, E. J.; Striebel, K.; McLarnon, F.; Andricacos, P. C. *Electrochim. Acta* **1987**, *32*, 355.
(80) Zhang, L.; Ma, C.; Mukerjee, S. *Electrochim. Acta* **2003**, *48*, 1845.
(81) Anderson, A. B.; Roques, J.; Mukerjee, S.; Murthi, V. S.; Markovic, N. M.; Stamenkovic, V. In preparation.
(82) Markovic, N. M.; Gasteiger, H. A.; Grgur, B. N.; Ross, P. N. *J. Electroanal. Chem.* **1999**, *467*, 157.
(83) Anderson, A. B.; Albu, T. V. *Electrochem. Commun.* **1999**, *1*, 203.
(84) Anderson, A. B.; Albu, T. V. *J. Am. Chem. Soc.* **1999**, *121*, 11855.
(85) Anderson, A. B.; Albu, T. V. *J. Electrochem. Soc.* **2000**, *147*, 4229.
(86) Kopitzke, R. W.; Linkous, C. A.; Nelson, G. L. *Polym. Degrad. Stab.* **2000**, *67*, 335.
(87) Buchi, F. N.; Gupta, B.; Haas; Scherer, G. G. *Electrochim. Acta* **1995**, *40*, 345.
(88) Scherer, G. G. *Ber. Bunsen-Ges. Phys. Chem.* **1990**, *94*, 1008.
(89) Hsueh, K. L.; Gonzalez, E. R.; Srinivasan, S. *Electrochim. Acta* **1983**, *28*, 691.
(90) Parthasarathy, A.; Srinivasan, S.; Appleby, A. J. *J. Electrochem. Soc.* **1992**, *139*, 2530.
(91) Paulus, U. A.; Wokaun, A.; Scherer, G. G.; Schmidt, T. J.; Stamenkovic, V.; Radmilovic, V.; Markovic, N. M.; Ross, P. N. *J. Phys. Chem. B* **2002**, *106*, 4181.